J. Fluid Mech. (1997), *vol.* 344, *pp.* 43–66. Printed in the United Kingdom

Numerical modelling of Coulomb-driven convection in insulating liquids

By R. CHICÓN[1], A. CASTELLANOS[2] AND E. MARTIN[1]

[1] Departamento de Fisica, Universidad de Murcia, Apdo. 4021, 30071 Murcia, Spain

[2] Departamento de Electrónica y Electromagnetismo, Facultad de Fisica, Avda. Reina Mercedes s/n, 41012 Sevilla, Spain

(Received 11 June 1996 and in revised form 17 March 1997)

Electroconvection in a layer of liquid subjected to unipolar injection is characterized by two stability criteria, a linear and a nonlinear one, with an associated hysteresis loop. Experimentally it is found that the velocity field fluctuates around its mean value. A temporal analysis of the measured current, which is directly related to the velocity, revealed the existence of a well-defined frequency correlated to the mean rotation time of a fluid particle in the convective cell, thus indicating that these fluctuations are not stochastic but related to the intrinsic dynamics of the system. Here a method of superparticles is used to solve the problem of the non-stationary electroconvection of the liquid. A good agreement between theoretical and experimental results is obtained.

1. Introduction

Flows driven by Coulomb forces are a common occurrence in many natural and industrial situations. Determination of the flow field and charge density distribution usually presents great difficulties, as the flow is influenced by the charge distribution through the electrical force term in the Navier–Stokes equation, which in turn is modified by the velocity field via the convection of charge. Fortunately, for those situations in which the Reynolds number is small, the velocity field may be expanded in a few modes. Typically one mode is enough to represent the flow with a few per cent of error (Atten & Lacroix 1979). The charge distribution on the other hand is strongly dependent on minute variations of the velocity field. For example, superimposing a small periodic component onto a cellular mean velocity field gives rise to chaotic mixing of the charge within the convective cell (Pérez & Castellanos 1991). In general, the charge density presents inner boundaries with sharp charge gradients. The complexity of the charge distribution makes impossible a modal analysis of the charge conservation equation with a reasonable number of modes. Owing to numerical diffusion, the usual finite elements or finite difference methods are not capable of resolving the small spatial and temporal scales present in the charge density distribution, even when specially designed antidiffusive schemes are used (Pérez & Castellanos 1989). Superparticle-type methods have to be resorted to, which amounts to substituting the partial differential equation for the charge density by thousands of ordinary differential equations, one for each superparticle (Hockney & Eastwood 1981).

In this paper we apply the superparticle method to the analysis of the finite-amplitude electroconvection of an insulating liquid layer subjected to unipolar injection. This is a paradigmatic case of Coulomb-driven convection in the

electrohydrodynamics (EHD) of isotropic liquids, equal in importance to the electroconvection in nematic liquid crystals (Dennin *et al.* 1996) and to the Rayleigh–Bénard problem in thermal convection, and has been the subject of much investigation during the last thirty years (for a review see Castellanos 1991 and Atten 1996). Controlling the charge injection by means of ion-exchange membranes allowed careful investigation of the electroconvection induced by strong injection from one of the electrodes. Experimentally, and theoretically, the existence of two stability criteria was determined: a linear one for the onset of motion, and a nonlinear one with an associated hysteresis loop in the current–voltage characteristics (Atten & Lacroix 1979). Experimentally, it was also found that finite-amplitude electroconvection is time dependent, with fluctuations of the velocity field around its mean value of a chaotic nature (Atten, Lacroix & Malraison 1980; Malraison & Atten 1982).

This time-dependent behaviour has until now defied any theoretical analyses, although this problem has been partially analysed in the case of weak injection (Pérez & Castellanos 1991). This analysis showed that even under smooth velocity fields the charge density distribution may be extraordinarily complex. To close the problem we need to be able to predict the velocity field and show that the steady finite-amplitude solution is unstable with a bounded solution for the velocity field. The complexity of the charge distribution precludes the possibility of finding analytical solutions, and numerical computations of this problem must be undertaken. A first attempt to solve this problem using a particle-type method was made by Castellanos & Atten (1987), and Castellanos, Atten & Pérez (1987). The case of weak unipolar injection was treated, and the existence of a long transient with chaotic fluctuations for the velocity was demonstrated. The actual Coulomb repulsion was replaced in the computation by the value corresponding to the hydrostatic solution, but as will be shown below, this ended in all time variations finally dying out. A preliminary study using the method of characteristics has already indicated that inclusion of the Coulomb repulsion could be enough to sustain the fluctuations (A. T. Pérez 1996, personal communication).

In this work, the superparticle method has been refined, and Coulomb repulsion is included by solving a Poisson equation at each time step. In this way we can show that the velocity fluctuations are present. The problem of arbitrary injection strength has been solved. In particular, the solution in the strong injection case makes it possible to compare our numerical simulations with known experimental results.

In the weak injection regime, where experimental results concerning time fluctuations are not yet available, the numerical results provide a range of relevant frequencies that may be explored to detect such fluctuations experimentally. Finally, the generality and flexibility of the method is shown through its application to a problem where the constraint of an autonomous injection is replaced by a more realistic field-dependent injection law in the weak injection regime (Felici & Gosse 1979; Pontiga, Castellanos & Malraison 1995).

2. Basic equations

An incompressible, isothermal and insulating liquid is considered, with density ρ, dynamic viscosity η and permittivity ϵ. It is confined between two parallel perfectly conducting plates of infinite extent, a distance d apart and with a constant potential difference ϕ_0 between them. Charge carriers of one sign are injected from one of the electrodes (unipolar injection), and migrate through the liquid with a velocity $K\boldsymbol{E}$, K being the ionic mobility and $\boldsymbol{E}$ the electric field. Unless the contrary is explicitly stated, it will be assumed that the injection is autonomous, i.e. that the charge density at the

injector remains constant and independent of the electric field. It is also supposed that the ions discharge instantaneously once they reach the opposite electrode.

The residual conductivity of the liquid is assumed to be very small (Atten & Lacroix 1979), typical values being less than $10^{-11}\ \Omega^{-1}\ \mathrm{m}^{-1}$. Therefore, the currents are small enough to allow neglect of magnetic effects as well as Joule heating in the electrohydrodynamic approximation (Melcher 1981). The electrical and mechanical equations may be written in non-dimensional form taking d, ϕ_0, $\epsilon\phi_0/d^2$ and $K\phi_0/d$ as the units for distance, potential, charge density and velocity, respectively:

$$\Delta\phi = -q, \tag{1}$$

$$\frac{\partial q}{\partial t} + \boldsymbol{\nabla}\cdot\boldsymbol{j} = 0, \tag{2}$$

$$\boldsymbol{\nabla}\cdot\boldsymbol{v} = 0, \tag{3}$$

$$\frac{T}{M^2}\left(\frac{\partial \boldsymbol{v}}{\partial t} + (\boldsymbol{v}\cdot\boldsymbol{\nabla})\,\boldsymbol{v} + \boldsymbol{\nabla}\tilde{p}\right) = \Delta\boldsymbol{v} + Tq\boldsymbol{E}, \tag{4}$$

where q denotes the charge density, ϕ the electric potential, $\boldsymbol{v}$ the velocity of the liquid and $\tilde{p}$ the sum of the mechanical and electrostriction pressures. The dielectric force term has been neglected in (4), as the permittivity is assumed to be constant throughout the liquid since Joule heating is negligible. The constitutive equation for the current density $\boldsymbol{j}$ is

$$\boldsymbol{j} = q(\boldsymbol{E} + \boldsymbol{v}), \tag{5}$$

where the first term accounts for the migration of the charge carriers due to the electric field and the second term accounts for the convection of charge by the liquid motion. The contribution of diffusion to the current can be ignored, since it is negligible compared with the migration term (Pérez & Castellanos 1989).

A coordinate system is chosen to add the appropriate boundary conditions, so that the (x, y)-plane coincides with the injecting electrode. Considering rigid electrodes results in the no-slip condition for the velocity, $\boldsymbol{v} = 0$ at $z = 0, 1$. The potential is fixed at the electrodes, so that $\phi(0) = 1$ and $\phi(1) = 0$. Finally, the assumption of autonomous injection provides an additional boundary condition at the injecting electrode, namely $q = C$ at $z = 0$.

Three non-dimensional parameters appear in the equations:

$$T = \frac{\epsilon\phi_0}{\eta K}, \quad C = \frac{q_0 d^2}{\epsilon\phi_0}, \quad M = \frac{1}{K}\left(\frac{\epsilon}{\rho}\right)^{1/2},$$

where q_0 is the charge density at the injector, T represents the ratio of the destabilizing Coulomb force to the stabilizing viscous force, C is a measure of the injection strength, and M is the ratio of the so-called hydrodynamic mobility of the ionic mobility. The character of $(\epsilon/\rho)^{1/2}$ as a hydrodynamic mobility can be easily understood by considering a complete conversion of the electric energy supplied to the system into kinetic energy of the liquid.

The equations admit a steady hydrostatic solution, with the charge density $q(z) = (a/2)(z+b)^{-1/2}$ decreasing from the injector while the electric field $E(z) = a(z+b)^{1/2}$, modified by the space charge, increases. The constants a and b depend on the injection strength C. This steady solution is potentially unstable (Atten & Moreau 1972), like the density distribution in the Rayleigh–Bénard problem, with T playing the role of the critical parameter. Above a critical value T_c, which corresponds to the linear stability criterion and depends on the injection strength C, the liquid is put into motion. The analogy with the Rayleigh–Bénard problem does not apply when the liquid is moving,

owing to the different physical mechanisms involved in the transport of the relevant scalar quantity at rest: heat is transferred by diffusion alone, whereas charge carriers move relative to the liquid with velocity KE. On the basis of simple physical arguments, it has been deduced that any stable motion of the liquid is characterized by a maximum velocity higher than KE (Felici 1969; Atten & Lacroix 1979). The motion organizes itself in the form of convective cells, the liquid flowing towards the injector in each cell with a velocity greater than the ionic drift velocity. Therefore, regions free of charge exist in each cell. This implies the existence of a nonlinear criterion T_f corresponding to finite-amplitude disturbances, smaller than T_c. Both solutions $\boldsymbol{v} = 0$ and $v_{max} > KE$ should be stable in the interval between the two criteria, giving rise to a hysteresis loop. This has been experimentally observed in the current–voltage curves in the space-charge-limited-current (SCLC) regime (Atten & Lacroix 1979).

The fluid motion will be assumed to be two-dimensional, in the form of self-similar rolls: $\boldsymbol{v} = A\boldsymbol{v}_0$, where $\max|\boldsymbol{v}_0| = 1$ and A is the amplitude. The velocity field $\boldsymbol{v}_0 = (v_0, w_0)$ is obtained from the stream function

$$\psi_0(x, z) = \frac{L}{2\pi}(1 - \cos 2\pi z)\sin\frac{\pi x}{L}, \tag{6}$$

so that $v_0 = \partial\psi_0/\partial z$ and $w_0 = -\partial\psi_0/\partial x$, the continuity equation being automatically satisfied. L is the half-wavelength of a convective cell, which is assumed to be equal to the value obtained from the linear stability analysis. Typical values that shall be used are $L = 0.687$ in the weak injection regime ($C = 0.1$), and $L = 0.614$ for strong injection ($C = 10$) (Atten & Moreau 1972). As long as T is close to the linear stability criterion T_c, this *a priori* velocity field is accurate to within a few percent.

The coupling existing between charge density and velocity field explicitly appears in the Navier–Stokes as well as in the charge conservation equations. Making the scalar product of (4) with $\boldsymbol{v}_0$ and integrating over the cross-section of a convective cell leads to the following equation for the amplitude $A(t)$:

$$\frac{T}{M^2}\left(\int_{cell}\boldsymbol{v}_0^2\,\mathrm{d}x\,\mathrm{d}z\right)\frac{\mathrm{d}A}{\mathrm{d}t} = \left(\int_{cell}\boldsymbol{v}_0\cdot\Delta\boldsymbol{v}_0\,\mathrm{d}x\,\mathrm{d}z\right)A + T\int_{cell}q\boldsymbol{v}_0\cdot\boldsymbol{E}\,\mathrm{d}x\,\mathrm{d}z. \tag{7}$$

The pressure and the nonlinear terms have a vanishing contribution to this averaged equation due to the symmetry conditions of the cell and the imposed velocity field $\boldsymbol{v}_0$. Equation (7) may be regarded as a balance between inertial effects, electric power and viscous dissipation. The constants appearing in the equation are readily evaluated as functions of the cell size L:

$$c_1 = \int_{cell}\boldsymbol{v}_0^2\,\mathrm{d}x\,\mathrm{d}z = \frac{L^3}{4} + \frac{3L}{16}, \tag{8}$$

$$c_2 = \int_{cell}\boldsymbol{v}_0\cdot\Delta\boldsymbol{v}_0\,\mathrm{d}x\,\mathrm{d}z = -\pi^2\left(L^3 + \frac{L}{2} + \frac{3}{16L}\right). \tag{9}$$

For a viscous-dominated regime, where inertial terms can be neglected, (7) reduces to

$$A(t) = -T\int_{cell}q\boldsymbol{v}_0\cdot\boldsymbol{E}\,\mathrm{d}x\,\mathrm{d}z\Big/\int_{cell}\boldsymbol{v}_0\cdot\Delta\boldsymbol{v}_0\,\mathrm{d}x\,\mathrm{d}z. \tag{10}$$

The last term in (7) contains the couple between charge density and liquid velocity. As will be discussed in more detail in §4, it is essential that sufficiently accurate charge and field distributions are used to evaluate this term.

Once $A(t)$ is determined, (1) and (2) have to be solved. The charge density is a

complex function of the velocity and no analytical solution is known for a time-dependent velocity amplitude. Any modal expansion of the charge is also excluded because of the strong charge gradients present in the system. For the same reasons, any numerical approach based on usual finite differences or finite elements is doomed to fail (Pérez & Castellanos 1989). Therefore, a direct method to solve the charge conservation equation has to be considered. The rest of this work is dedicated to the development and application of a particle-type method designed to accomplish this aim.

3. The particle-type method

In the charge conservation equation the true discrete charge carriers are replaced by a continuum fluid of charge, where the graininess of the charge is smoothed out. The discretization of this equation leads to the concept of computational superparticles, which can be thought of as clouds of ions (Hockney & Eastwood 1981). These superparticles possess a conserved attribute, the electric charge, and other variable attributes, position and velocity. Thus, conservation of charge is automatically satisfied, while the variable attributes evolve according to the equations of motion whose driving terms obey the field equations.

Simulation of the physical system proceeds as follows. A number of charged superparticles are injected at one of the electrodes, simulating the true ions and conserving the charge all along its motion. The equations of motion for the superparticles are

$$\frac{\mathrm{d}\boldsymbol{r}_i}{\mathrm{d}t} = A(t)\,\boldsymbol{v}_0 + \boldsymbol{E}, \tag{11}$$

where $\boldsymbol{r} = (x, z)$, $\boldsymbol{v}_0$ is the self-similar velocity field given by (6) and $A(t)$ is the time-dependent amplitude. $\boldsymbol{E}$ represents the total electric field, including the Coulomb interaction between the ions. The equations of motion are integrated numerically using a fourth-order Runge–Kutta method.

The electric field at each time is obtained from a Poisson equation for the potential. In order to solve this equation it is necessary to revert from the discrete model involving charged superparticles to a continuum charge density distribution. Field quantities such as electric potential, electric field and charge density are represented by their values at a regular array of mesh points. The first step consists in assigning the charge of the superparticles to their nearby mesh points in order to have a mesh-defined charge density. Then, solving the Poisson equation numerically gives the values of the potential at the mesh points, from which the values of the electric field are readily obtained. Finally, the electric field at the superparticle positions is calculated by interpolating the mesh-defined field values. Since both particle and mesh features are present, the method can be classified within the category of particle-mesh methods (Hockney & Eastwood 1981).

The charge assignment procedure can be described as follows. The charge of a superparticle must be distributed among the nearby mesh points according to a well-defined prescription, so that the charge density q_p at a mesh point $\boldsymbol{r}_p$ is given by

$$q_p = \frac{1}{V_p} \sum_{i=1}^{N_p} W(\boldsymbol{r}_i - \boldsymbol{r}_p)\, Q_i, \tag{12}$$

where the sum extends over the total number N_p of particles, V_p is the volume of the corresponding mesh cell, Q_i the charge of superparticle i located at $\boldsymbol{r}_i$ and $W(\boldsymbol{r}_i - \boldsymbol{r}_p)$ represents the fraction of the charge Q_i assigned to $\boldsymbol{r}_p$, which is a function of the position of the superparticle relative to the mesh point. A very accurate assignment

scheme is that known as the *cloud in cell* (CIC), which involves the four nearest neighbours to a superparticle, and the corresponding function $W(\boldsymbol{r}_i - \boldsymbol{r}_p)$ is (Hockney & Eastwood 1981)

$$W(\boldsymbol{r}) = \begin{cases} (1-|x|/h_x)(1-|z|/h_z) & \text{if } (x,z) \in [-h_x, h_x] \times [-h_z, h_z] \\ 0 & \text{otherwise,} \end{cases} \tag{13}$$

where h_x and h_z are the horizontal and vertical distances between the four adjacent mesh points that define the square containing the superparticle. The CIC scheme allows a simple intuitive geometrical interpretation, as shown in figure 1(*a*).

Once the charge density is available, the Poisson equation is solved numerically using a finite-differences scheme. The appropriate boundary conditions for the potential correspond to the fixed values at the electrodes, together with the assumption that L corresponds to half a wavelength. This implies that the x-component of the electric field vanishes at the vertical boundaries of the cell, i.e. $\partial\phi/\partial x = 0$ at $x = 0$ and $x = L$. The resulting linear system is solved by a direct block elimination method (Isaacson & Keller 1966). The electric field is finally obtained from the potential by central differences.

The final step in the particle-mesh calculation is interpolation of the mesh-defined electric field values to find the field acting on the superparticles. Arguments based on physical grounds are in favour of the same force interpolation and charge assignment schemes (Hockney & Eastwood 1981). The electric field at a superparticle position $\boldsymbol{r}_i$, is then evaluated as

$$\boldsymbol{E}(\boldsymbol{r}_i) = \sum_{p=1}^{N_g} W(\boldsymbol{r}_i - \boldsymbol{r}_p)\, \boldsymbol{E}(\boldsymbol{r}_p), \tag{14}$$

where the sum extends over all the N_g mesh points and $\boldsymbol{E}(\boldsymbol{r}_p)$ are the mesh-defined values of the field. The function W is that corresponding to the CIC scheme, (13).

Summarizing, the main steps in the particle-mesh calculation are the following:

(i) assign charge to the mesh from a given configuration of the superparticles in the system;

(ii) solve the Poisson equation for the potential, and calculate the electric field;

(iii) interpolate the electric field at the superparticle positions;

(iv) move the superparticles with the current value of the electric field and liquid velocity field, to get a new configuration of the system;

(v) calculate a new value of the amplitude $A(t)$ consistent with the new configuration of the system, according to (7) or (10).

Thus, given a sequence of time levels $t_n = n\,\Delta t$, $n = 0, 1, \ldots$, the corresponding values of the velocity amplitude are obtained as

$$A_{n+1} = A_n + \frac{M^2}{Tc_1}\left(c_2 A_n + T \int_{cell} q^{n+1} \boldsymbol{v}_0 \cdot \boldsymbol{E}^{n+1}\, \mathrm{d}x\, \mathrm{d}z\right)\Delta t \tag{15}$$

if (7) is used, or

$$A_{n+1} = -\frac{1}{c_2} T \int_{cell} q^{n+1} \boldsymbol{v}_0 \cdot \boldsymbol{E}^{n+1}\, \mathrm{d}x\, \mathrm{d}z \tag{16}$$

in the case of a viscous-dominated regime ($M = \infty$), equation (10). The charge density and electric field previously computed in steps (i) and (ii) at time t_{n+1} are used to evaluate the integral in (15) or (16), using the trapezoidal rule (Press *et al.* 1986).

Although it is clear from physical reasons that the current circulating through the cell should be closely related to the liquid velocity, it is worth calculating the current as well as the amplitude of the velocity field. The experimentally measured electrical

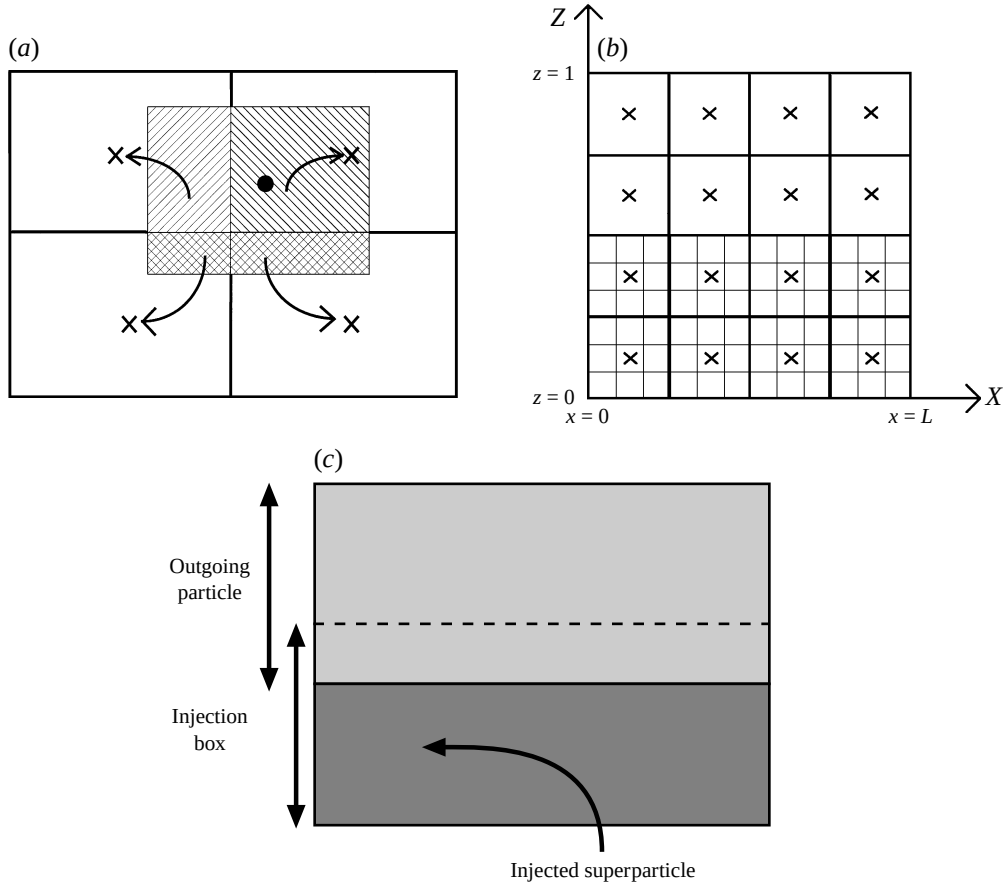

FIGURE 1. (*a*) The CIC assignment scheme. The fraction of charge assigned to the four neighbouring mesh points from a particle (located at the position represented by the dot) is proportional to the area of overlap of the particle cloud (hatched square) with the cells containing those mesh points. (*b*) Mesh points (crosses) and an initial tesselation of the computational cell with superparticles. The boxes contiguous to the injector are the *injection boxes*. (*c*) Schematic representation of the injection mechanism.

current (in non-dimensional units and per unit length in the y-direction) corresponds to

$$\int_{z=\text{constant}} \left[q(Aw_0 + E_z) + \frac{\partial E_z}{\partial t} \right] \mathrm{d}x, \tag{17}$$

which is readily shown to be independent of z from Ampère's law and the boundary conditions in the cell. It is important to include the displacement current, even though its magnitude is usually quite small compared to the current due to the flow of charge (at most 1/30 of the flow current in the results presented in the next Section), because its time dependence significantly contributes to the actual time fluctuations of the current. The integral in (17) is numerically computed at time t_n on every horizontal plane of the mesh and the average over all the planes is taken as the value of the current, smoothing out as much as possible the computational errors inherent in the mesh.

A crucial question in the construction of the computational model is concerned with the role of the boundary conditions. Some of them have already been taken into account: those referring to the fluid are explicitly included in the self-similar velocity

field considered, and those affecting the electric potential are employed in the numerical solution of the Poisson equation. Only the autonomous injection hypothesis remains to be analysed. The injection mechanism used in the simulation is described in the following.

Let us consider an initial configuration of the system, consisting of a tesselation of the whole computational cell with a number of superparticles, say $n_1 \times n_2$ superparticles in each mesh cell, that without any loss in generality are supposed to be rectangular as shown in figure 1(*b*). The state corresponding to the steady hydrostatic solution is obtained by giving the appropriate charge to each superparticle. The grid elements adjacent to the injecting electrode will be considered *injection boxes*, where the boundary condition on the charge density is to be satisfied. A new superparticle is introduced into each injection box at each step, to compensate for the charge loss as the particles occupying the injection boxes in the previous step move away from the injector, driven by the electric field (figure 1*c*). In this way the number of particles adjacent to the injector is kept constant. Since the fraction of charge leaving each injection box when the particles are moved is proportional to the time step Δt, the charge of the injected particles is also proportional to Δt. Therefore, any variation of the electric field at the injector will result in different values for the charge of the injected particles. This simple injection mechanism has proved to be very efficient in complying with the autonomous injection hypothesis. Moreover, it can be implemented without any additional difficulty whatever the injection law, as will be shown in the next Section. As regards the ejection mechanism, the ions discharge instantaneously when they reach the collector. In the computational model this simply means that superparticles are removed from the system when this occurs.

The number of superparticles in the system is essentially dependent on the timestep Δt and the number of injection boxes. This is easily understood since all the superparticles injected at a given place will take the same time on average to reach the collector. Hence, the number of superparticles present at a given time and coming from a given injection box will be on average equal to the number of timesteps corresponding to the crossing time. Thus, the timestep as well as the number of injection boxes have to be carefully established. The timestep should be small enough so that a superparticle next to the injector moves a distance less than the size of the injection box, and the number of injection boxes should be sufficient to avoid the spurious fluctuations of mesh-defined quantities, but always keeping the total number of superparticles within reasonable computational capabilities.

4. Results and discussion

4.1. *The steady hydrostatic solution*

The validity and accuracy of the particle method described in the previous Section is first checked by application to the steady hydrostatic state, where comparison with the analytical solution is possible. In this case the velocity of the liquid is taken to be zero, and all steps of the particle-mesh method are performed, except the last one that calculates the amplitude of the velocity field.

Two different regimes have been considered: the weak injection regime, with a typical value of $C = 0.1$, and the strong injection regime (SCLC), with values of around $C = 10$. There is no substantial difference in the application of the method in the two regimes, except for one technical, but crucial, point. In the weak injection regime the steady hydrostatic charge density and electric field distributions show a very slow variation with the z-coordinate (Atten & Moreau 1972). Thus, a regular mesh will be

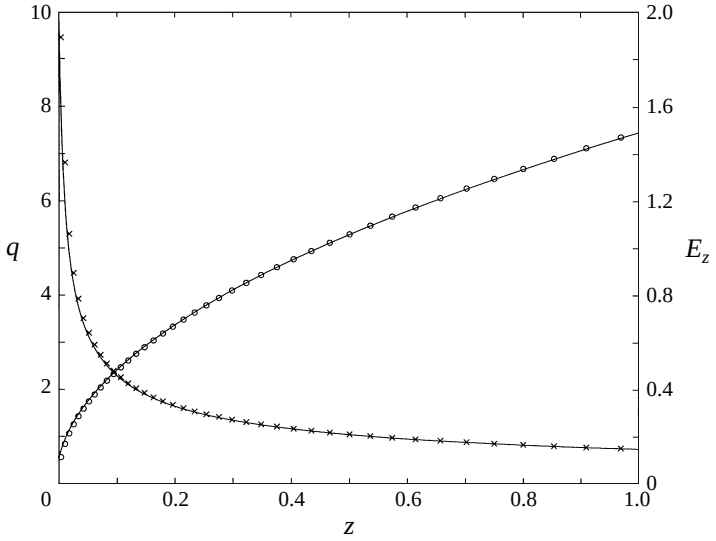

FIGURE 2. Charge density (crosses) and electric field (circles) in the steady hydrostatic state for strong injection ($C = 10$). The timestep is $\Delta t = 1/300$.

a correct choice for the particle-mesh calculation. On the other hand, in the SCLC regime both charge density and electric field show drastic variations near the injector (Schneider & Watson 1970; Atten & Moreau 1972). In the limit, the electric field is zero and its derivative, the charge density, tends to infinity at $z = 0$. Such strong gradients in the z-coordinate in a region so close to the injector are not consistent with using a regular mesh in the particle-mesh calculations.

In the weak injection case the mesh consists of $N_1 \times N_2$ equal cells, with size $h_x = L/N_1$ and $h_z = 1/N_2$ in the x- and z-directions, respectively. The mesh points are located at the centre of the cells (figure 1*b*). It is assumed that $n_1 \times n_1$ superparticles initially fill each mesh cell, and hence the number of injecting boxes is $N_1 \times n_1$. For $C = 0.1$, taking $N_1 = 30$, $N_2 = 30$, $n_1 = 4$, $n_2 = 3$ and $\Delta t = 1/200$, the deviations of numerical from analytical results for the hydrostatic solution do not exceed 1%. The small discrepancy is basically attributable to the charge assignment procedure used, so representing to a certain extent a measure of the accuracy of the method. Some small static fluctuations can be observed in the computed charge density when the timestep is $\Delta t = 1/200$. This is entirely due to the discrete character of the time levels, and the fluctuations disappear when a smaller Δt is used. The fluctuations are much smaller in the electric field, which is consistent with the field being an integral of the charge density. It has also been checked that by doubling the number of mesh points the deviations from the analytical results decrease by approximately a factor two, and the first-order approximation of the overall method is confirmed. As the transit time of an ion from one electrode to the other is of the order of unity, the number of superparticles involved in the calculation of the steady state is approximately the number of injection sites divided by the timestep, which gives around 24000 superparticles when $\Delta t = 1/200$. This number is large enough to prevent the appearance of spurious fluctuations in the mesh-defined quantities. Some technical details concerning the particle-mesh calculations can be found in the Appendix.

In the strong injection regime a non-uniform mesh must be employed, as mentioned above. The method followed to construct this mesh is explained in the Appendix. The charge density and electric field distributions corresponding to the hydrostatic solution

are shown in figure 2, for an injection strength $C = 10$. The results have been obtained using a mesh with $N_1 = 30$, $N_2 = 40$, $n_1 = 4$ and $n_2 = 3$, and a timestep $\Delta t = 1/300$. The transit time of the ions may be evaluated easily from the analytical expression for the electric field, and it turns out to be larger than in the weak injection regime. This results in a considerable increase in the number of superparticles present in the system, which, in the case considered, is about 45700.

4.2. *The linear stability criterion*

Whereas the velocity field of the liquid was 'turned off' in the problem considered in the previous subsection, the self-similar velocity field corresponding to (6) is now 'turned on', and the ions are driven by the sum of the electric and velocity fields. Starting from the steady hydrostatic solution reached previously, the system is subjected to a small perturbation. The amplitude $A(t)$ of the velocity field is then calculated at time levels $t_n = n\Delta t$, using either (15) or (16). This is done for a fixed value of C and varying the parameter T. For sufficiently low values of T, the amplitude $A(t)$ dies out, and the steady (purely conductive) hydrostatic state is reached. When T is above a critical value T_c, the velocity amplitude starts to grow, very slowly at first and then much more quickly, as the charge distribution begins to differ appreciably from that of the hydrostatic solution. Once the amplitude $A(t)$ reaches a value greater than the electric field some regions of the computational cell become inaccessible for the ions coming from the injector. The amplitude shows very large fluctuations, until it finally stabilizes with small fluctuations around a finite average value. Two typical cases are shown in figure 3.

The critical value T_c gives the linear stability criterion. In a typical case within the weak injection regime, with $C = 0.1$, the result obtained is $T_c = 23450$. This value has been computed for several values of the parameter M($M = \infty$, 200, 100, 50 and 20) and is found to be independent of M as expected. In the strong injection regime, $C = 10$, for instance, $T_c = 171$, again independent of the value of M ($M = \infty$, 40, 20, 10 and 5 were used in the calculation). These results show very good agreement with those theoretically predicted by the linear stability analysis (Atten & Moreau 1972), and represent an improvement over previous numerical results obtained in the weak injection regime by two different methods: a finite difference method and a particle-type method (Castellanos & Atten 1987).

4.3. *Time-dependent finite-amplitude electroconvection*

4.3.1. *Weak injection regime*

The motion of the liquid organizes itself above the stability threshold with a finite average velocity amplitude greater than the migration velocity of the ions, as was already predicted by the simple hydraulic model of weak unipolar injection developed by Felici (Felici 1969; Atten & Lacroix 1979). An important consequence is that a certain region of the cell cannot be reached by the ions, and hence is void of charge. The charge distribution in the cell is readily obtained for a given value of the velocity amplitude if Coulomb repulsion between the ions is neglected, since in this case the charge density remains constant along the ion trajectories (Pérez & Castellanos 1991). For $A > 1$ the convective cell is divided into two unconnected regions: one containing the trajectories of the injected ions joining the injector and the collector with a constant charge density C, the other corresponding to closed orbits and therefore strictly free of charge. Both regions are separated by a curve referred to as the *separatrix*. The empty region represents a major part of the cell when $T > T_c$ due to the very large value of the velocity, as can be seen in the plots of the charge density (figure 4), in which it can

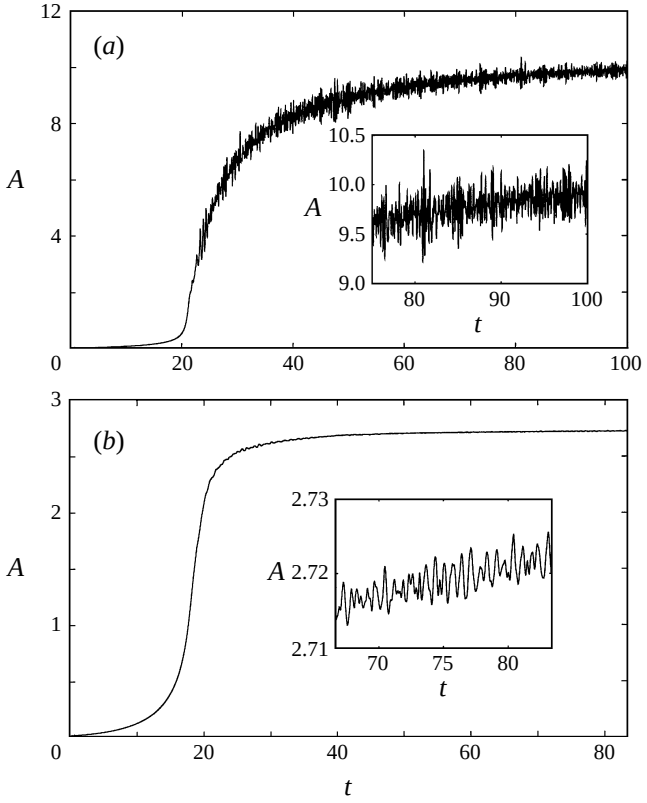

FIGURE 3. Time evolution of the velocity amplitude. (*a*) Weak injection ($C = 0.1$, $T = 24000$). (*b*) Strong injection ($C = 10$, $T = 178$).

also be observed that a small amount of charge is found inside the almost empty region in the cell. The almost charge-free region becomes smaller for subcritical values of T, since the velocity amplitude is lower, and also the amount of residual charge found in that region is smaller.

The critical value T_f of the nonlinear criterion and the corresponding hysteresis loop for the velocity are shown in figure 5. The result obtained for the nonlinear criterion, $T_f/T_c C = 0.87$, and the asymptotic behaviour agree well with the predictions of the approximate analytical solution, $T_f = 0.93 T_c C$ and $A \sim T^{1/2}$ for large T (Castellanos & Atten 1987).

It has been found that both the velocity and the charge density fluctuate in time, the velocity fluctuations sustaining the charge fluctuations via (2) and the latter sustaining the former via (4). This is at variance with previous computations, for which the fluctuations in the velocity amplitude finally disappeared and part of the cell ended up strictly free of charge (Castellanos & Atten 1987; Castellanos *et al*. 1987). The new physical feature which is taken into account is an accurate calculation of the actual Coulomb repulsion, instead of considering a mean field corresponding to, or similar to that of, the hydrostatic state. Two facts of physical interest, essentially linked to each other, stem from this approach: the time fluctuations of velocity and current, and the existence of a small amount of charge inside the hole in the cell. It has also been verified that less marked changes in the field, such as a homothetic transformation with a dilatation factor not far from unity applied to the solution of the Poisson equation, can completely destroy the time behaviour shown in figure 3.

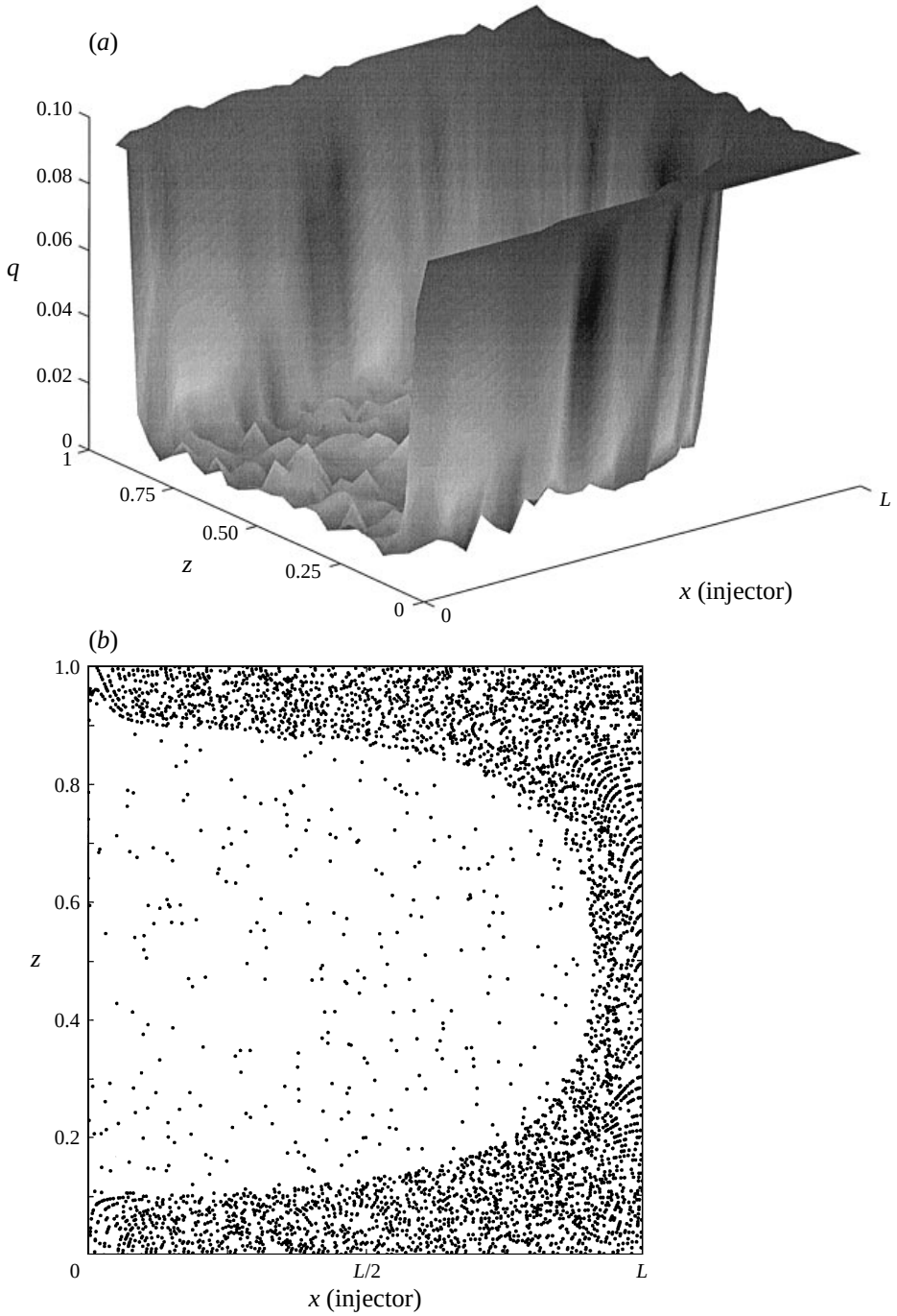

FIGURE 4. Charge density distribution for weak injection above the stability threshold ($C = 0.1$, $T = 24000$). (*a*) Three-dimensional plot; (*b*) cross-section of the computational cell, where the positions of 5000 randomly chosen superparticles have been plotted.

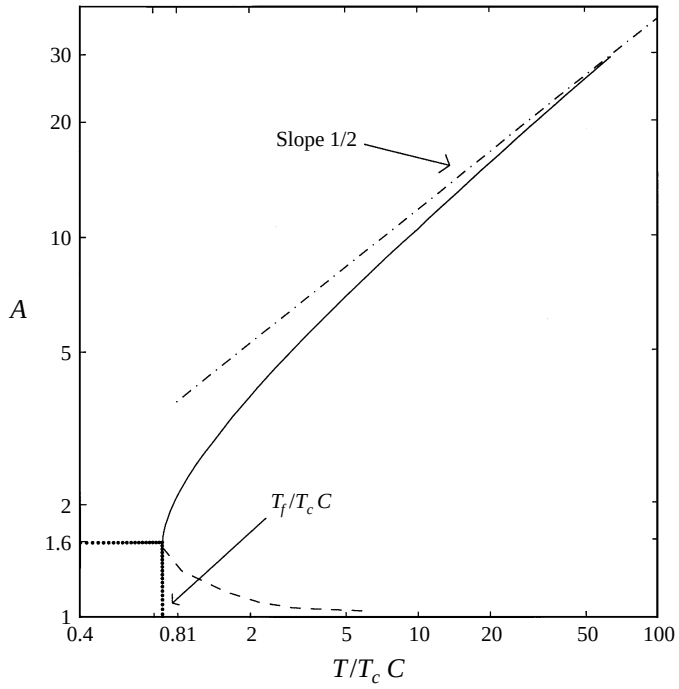

FIGURE 5. Velocity amplitude as a function of $T/T_c\,C$ for weak injection ($C = 0.1$). The nonlinear criterion is $T_f = 0.87T_c\,C$, with $A = 1.6$.

It was already noticed in a previous work (Pérez & Castellanos 1989) that if the Coulomb repulsion was included a region connecting the hole with the collector appeared, thus providing an escape route for the charges. This channel has been detected numerically, and was found to be very narrow with a width that fluctuates with time. The maximum width has been found to be of the order of 1/90 of the horizontal size of the convective cell, which shows that the dynamics is governed by the behaviour of the ion trajectories near the unperturbed separatrix, in agreement with the theoretical results obtained for a time-dependent amplitude $A = A_0 + \epsilon \sin(\Omega t)$ in the weak injection regime (Pérez & Castellanos 1991). This theoretical analysis demonstrated the existence of a chaotic layer around the separatrix, causing a mixing of charge that substantially modifies the charge density distribution.

While the average value of the velocity is independent of M for a given value of T, as is to be expected from (7), the amplitude of the velocity fluctuations is not, as shown in figure 6. With $C = 0.1$ and $T = 23\,800$, slightly above the instability threshold, it varies from about 2% of the average value of the velocity for $M = \infty$ to 0.5 per thousand for $M = 20$ (the results are practically identical for $M = \infty$ and $M = 200$). For $T = 10\,000$, well below the linear criterion, the fluctuations range from about 6 per thousand for $M = \infty$ to 0.6 per thousand for $M = 20$. The increase of fluctuations with M may be understood on a physical basis, since large values of M correspond to lower mobilities, which means that the ions are more strongly dragged by the liquid and can therefore be more easily trapped in the separatrix. The same conclusion can be reached in a somewhat more formal way through a simple analysis of the evolution equation for the fluctuations, that can be readily obtained from (7). In a first approximation, replacing the fluctuating time-dependent forcing term that appears in this equation by an oscillatory forcing term leads to an oscillatory solution for the fluctuations, with an

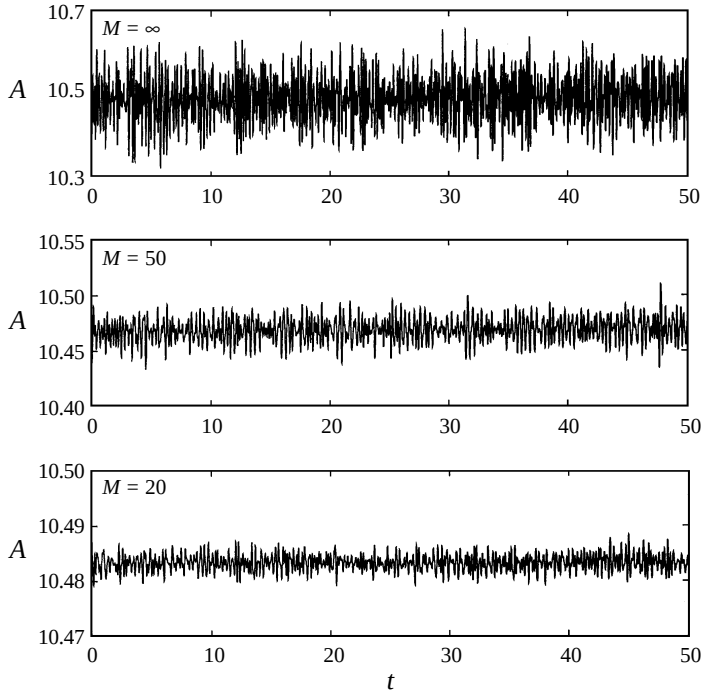

FIGURE 6. Time fluctuations of the velocity in the weak injection regime ($C = 0.1$, $T = 23\,800$) for different values of $M (M = (\epsilon/\rho)^{1/2}/K$ is the ratio of the hydrodynamic mobility to the true ionic mobility). Note the change of scale in the plots.

amplitude that increases with M. Although no quantitative prediction about the amplitude of the fluctuations could be expected from this rough approximation, it yields the right qualitative behaviour of the fluctuations with M.

The time behaviour of the current, computed according to (17), very closely resembles that of the velocity amplitude, as expected on physical grounds. Despite the lack of experimental data concerning the current fluctuations in the weak injection regime, it would seem interesting to analyse their magnitude and spectral characteristics. The amplitude of the current fluctuations varies from about 2% of the average value of the current for $M = \infty$ to 1% for $M = 20$ when $T = 23\,800$, and from 6 per thousand for $M = \infty$ to 3 per thousand for $M = 20$ when $T = 10\,000$.

Some of the experimental features of the power spectra found in the SCLC regime are also encountered numerically in the weak injection case. The power spectra for the velocity, shown in figure 7, and the current are entirely similar. A broadened peak appears around a frequency f_1, basically independent of M, followed by an exponential decay with a characteristic frequency f_c. The peak frequency f_1 is directly related to the average value of the liquid velocity (Malraison & Atten 1982). In fact, f_1 corresponds very closely with the mean rotation time of a fluid particle in the convective cell. The behaviour of f_1 and the ratio f_c/f_1 with the voltage are shown in figure 8, and they exhibit very similar features to those found in the SCLC regime. Typical values of f_1 are expected to be between 70 and 400 Hz under experimental conditions similar to those discussed in Pontiga *et al.* (1985). It would be of interest to measure these high-frequency fluctuations. The apparatus employed to measure the current should respond to these frequencies, and any standard data acquisition system would then make it possible to verify the existence of the fluctuations.

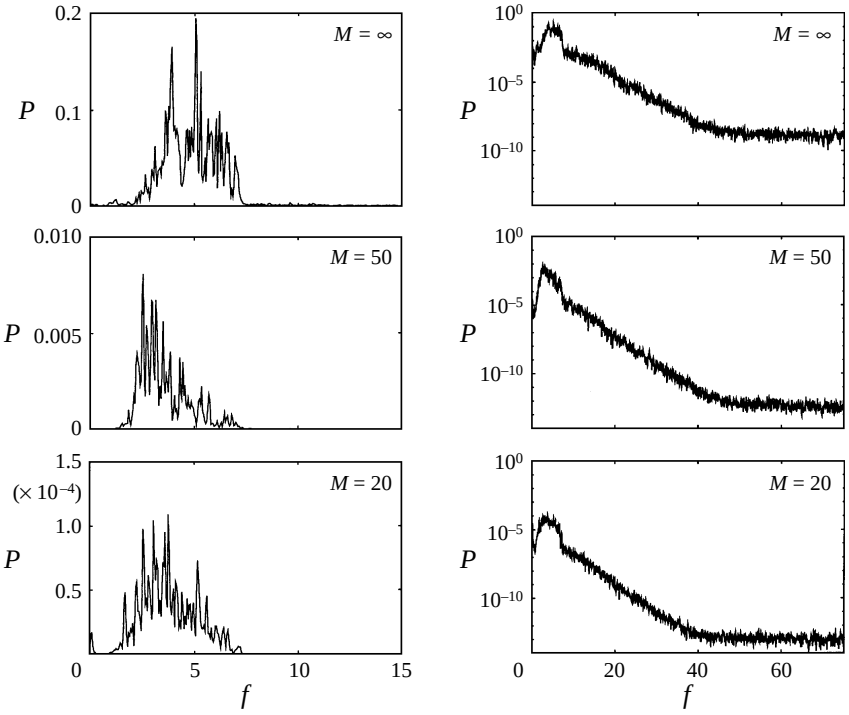

FIGURE 7. Linear and logarithmic plots of the power spectral density of the velocity fluctuations as a function of frequency, in the weak injection regime ($C = 0.1$, $T = 23\,800$), for different values of M.

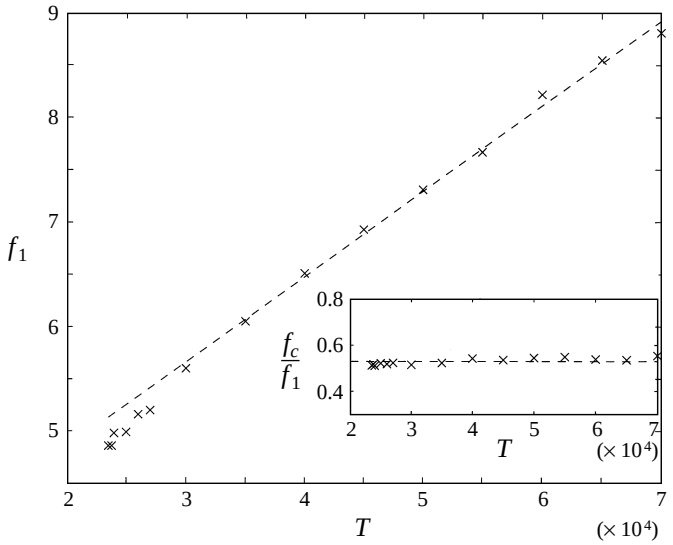

FIGURE 8. Peak frequency f_1 as a function of T for weak injection ($C = 0.1$, $M = \infty$). Inset: the ratio f_c/f_1 versus T. f_c is the characteristic decay frequency.

4.3.2. *Strong injection (SCLC) regime*

The charge distribution in the convective cell is shown in figure 9 for a value of T slightly above the stability threshold. It is apparent from the figure that the size of the hole is now less than in the case of weak injection, according to the much lower values

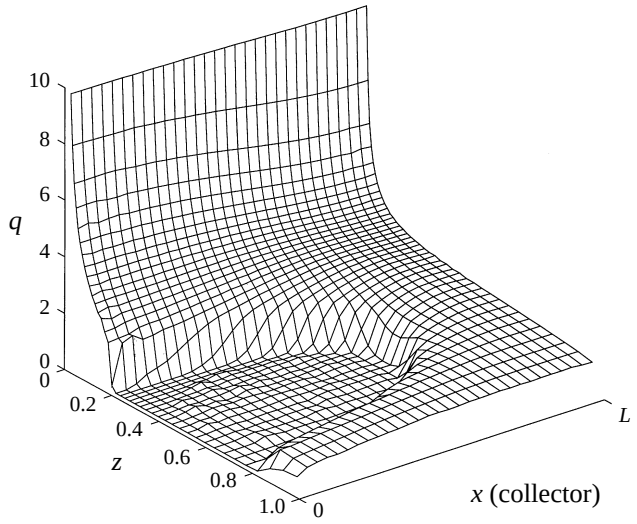

FIGURE 9. Charge density distribution for strong injection above the stability threshold ($C = 10$, $T = 185$).

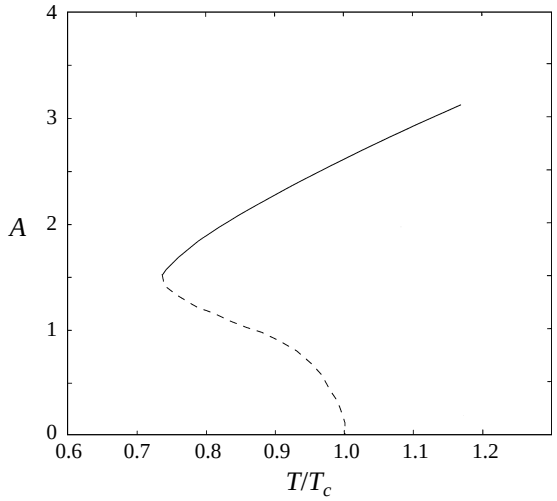

FIGURE 10. Velocity amplitude as a function of T/T_c for strong injection ($C = 10$). The nonlinear criterion is $T_f = 0.74T_c$, with $A = 1.5$.

of the liquid velocity above the linear stability criterion in the SCLC regime. The nonlinear criterion T_f and the hysteresis loop obtained for the average velocity are shown in figure 10. The results are in good agreement with those obtained in a previous work using a Galerkin method (Atten & Lacroix 1979).

The previous discussion on the close relation between the time fluctuations of velocity and current and the existence of a small amount of charge in the hole applies without changes to the results obtained in the SCLC regime. The relative amount of charge in the hole is now smaller than in the case of weak injection. This may be understood on the basis of the relation $(1-\beta)/\beta^2 = C_b/\delta$, where C_b is the average value of the charge density near the border of the hole, βC the average charge density inside the hole, and δ a typical distance associated with the charge gradient (Pérez &

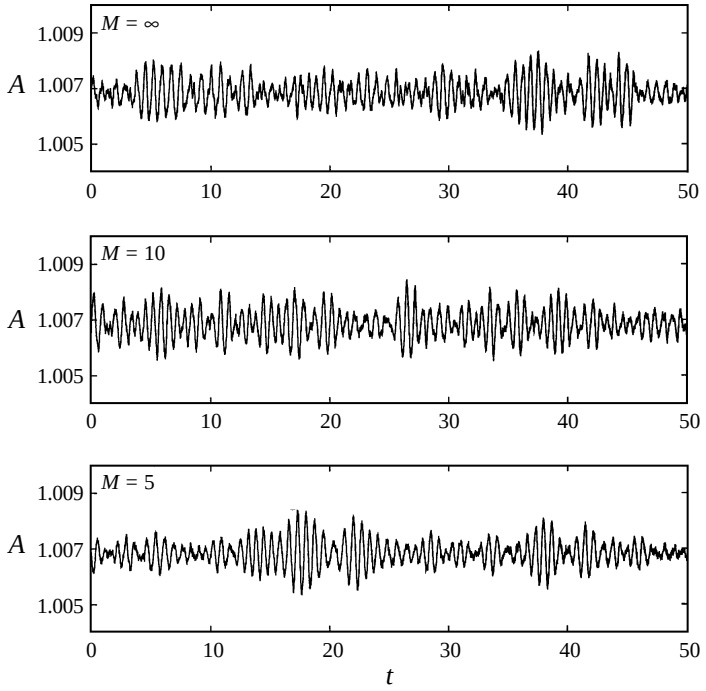

FIGURE 11. Time fluctuations of the current (in non-dimensional units) in the strong injection regime ($C = 10$, $T = 178$) for different values of M.

Castellanos 1989). Typically $\delta \approx 10^{-2}$, $C_b \approx C/5$ for $C = 10$ (see figure 9) and $C_b \approx C$ for weak injection (see figure 4). This rough estimation gives $\beta \approx 0.3$ for $C = 0.1$, and $\beta \approx 0.07$ for $C = 10$, which are of the order of the results obtained in the simulation. Consequently, the amplitude of velocity and current fluctuations relative to their average value is also notably smaller than it was for weak injection, as may be seen from figure 11. For $C = 10$ and $T = 178$, slightly above the instability threshold, the velocity and current fluctuations range from about 3 per thousand for $M = \infty$ to 2 per thousand for $M = 5$, and from 2 per thousand for $M = \infty$ to 1 per thousand for $M = 5$, respectively ($M = 20$ is practically infinity in this case). Below the linear criterion, for $C = 10$ and $T = 140$, the fluctuations exhibit less sensitivity to the value of M, being of the order of 2 per thousand for the velocity and 0.8 per thousand for the current. These results are well within the range of the experimental results (Malraison 1984). The existence of a narrow channel connecting the hole with the collector has also been confirmed by the computational results in the SCLC regime.

Some characteristic power spectra of velocity and current are shown in figure 12. They all present an enlarged peak at a characteristic frequency f_1, independent of M, that increases with the voltage, as can be seen in figure 13, where the non-dimensional frequency is plotted versus T. These results are in fairly good agreement with the experimentally observed relation $f_1 \propto \phi_0^2/d^2$ (Atten *et al.* 1980; Malraison & Atten 1982), since T is proportional to the voltage. A region of exponential decay with frequency can be clearly observed in the power spectra of the velocity, though it is much less apparent in the current spectra except at higher voltages. The ratio between the characteristic frequency f_c of the exponential part of the spectra and f_1 is also plotted in figure 13. It is always near 0.42, a value lower than the 0.7 of the experimental results discussed in Malraison & Atten (1982).

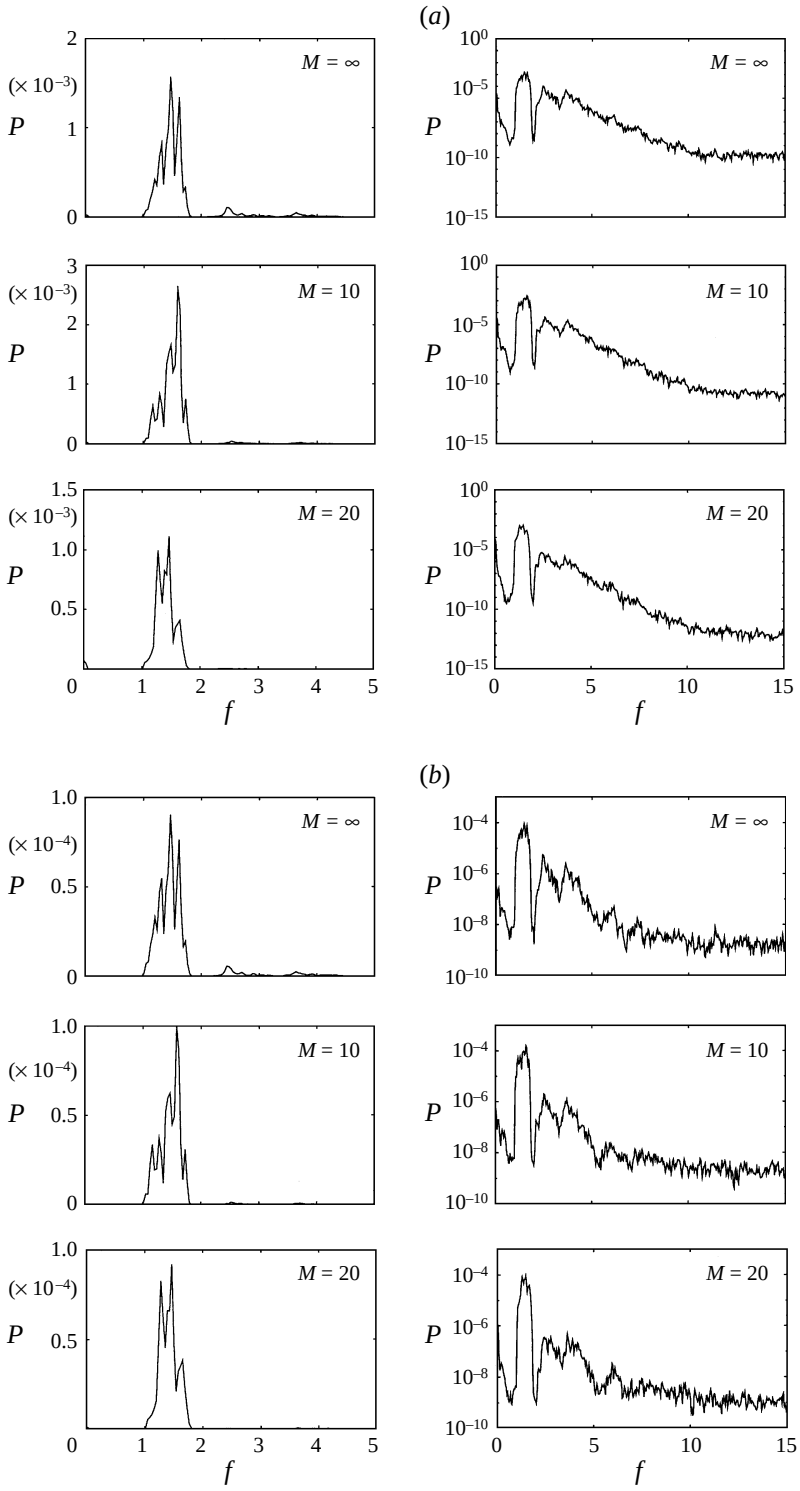

FIGURE 12. Power spectral density of the fluctuations in the velocity (*a*) and the current (*b*) as a function of frequency for strong injection ($C = 10$, $T = 178$), for different values of M.

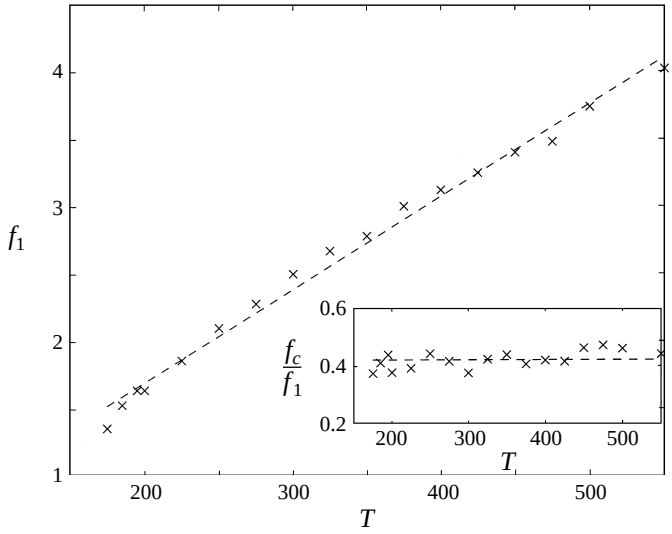

FIGURE 13. Peak frequency f_1 as a function of T for strong injection ($C = 10$, $M = \infty$). Inset: the ratio f_c/f_1 versus T. The characteristic decay frequency f_c has been obtained from the velocity spectra.

4.4. *Computer simulation of experiments*

The particle method described in this paper was used to simulate some real experimental situations. The experimentally well-known strong injection regime will be considered first.

4.4.1. *Strong injection regime*

Always assuming an autonomous injection, a voltage ϕ_0 below the stability threshold is initially established, and then gradually increased while the separation between the electrodes is kept constant, the system being allowed to reach the steady hydrostatic state at each step. Two experimental conditions have been considered with different injection strengths. In the first one the initial voltage ϕ_0 is chosen to correspond to $T = 100$ and $C = 10$. In the second, with the lower injection strength, the initial voltage corresponds to the same value $T = 100$ but with a lower value of $C = 7$. The two parameters T and C vary when the voltage ϕ is changed, according to the hypothesis that q_0 remains constant. The computed electrical current density accurately follows the theoretical law $J = (9/8)\,\epsilon K\phi^2/d^3$ for motionless liquids in the SCLC regime (Schneider & Watson 1970), as shown in figure 14.

The current experiences a sudden discontinuity when the linear stability criterion $T = T_c$ is reached. The critical values obtained are $T_c = 173$ ($C = 5.8$ at the critical voltage) in the first case and $T_c = 193$ ($C = 3.6$ at the critical voltage) in the second, which compare very favourably with the theoretical predictions of the linear stability analysis (Atten & Moreau 1972). It is also found that the higher the injection strength, the larger the jump in the current, amount to about 40 % of the value of the current below the threshold in the first case, and 35 % in the second. The steeper slope in the plot of the current versus the square of the voltage above the instability threshold found in the experimental results (Atten & Lacroix 1979), has been also obtained numerically.

The hysteresis loop is obtained by decreasing the voltage from above the threshold. The motion of the liquid is sustained until a new critical value of the voltage, lower

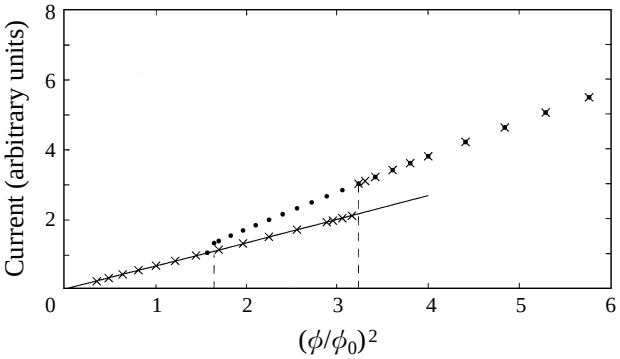

FIGURE 14. Current as a function of the square of the voltage in the strong injection regime. $C = 10$ and $T = 100$ when $\phi = \phi_0$. The crosses and dots correspond to increasing and decreasing voltages, respectively, and the solid line to the theoretical law $J = (9/8)\,K\epsilon\phi^2/d^3$.

than the former value, is reached, which corresponds to the nonlinear criterion T_f. The values obtained are $T_f = 125$ ($C = 8$ at that voltage) in the first case and $T_f = 130$ ($C = 5.4$ at that voltage) in the second, in reasonable agreement with the numerical results obtained with a Galerkin method (Atten & Lacroix 1979). A new jump in the current, smaller than the previous one, takes place, and the steady hydrostatic state is recovered again. The relative magnitude of this jump is around 17 and 15% in the two cases, respectively. Typical experimental values for the jumps in the current (Atten & Lacroix 1979) are much smaller than those obtained in this work with the particle method. However, it should be noted that the critical voltages obtained numerically, especially for the linear criterion, are overestimated with respect to the experimental values not only when obtained by the method developed in this work but also in previous attempts (Atten & Lacroix 1979). If the appropriate correction factors for the critical values of T are considered, the jumps in the current become equal in size to the experimental results.

It is worth noticing that the electric field near the injecting electrode noticeably increases when the liquid is put into motion. This fact must be taken into account when choosing a suitable timestep and mesh size near the injector.

4.2.2. *Weak injection regime*

As suggested in Pontiga *et al.* (1995), the detection of the linear instability threshold in the weak injection regime should be carried out at a fixed voltage and varying the electrode separation, exactly the opposite of what is done in the case of SCLC. Therefore, the computational experiment will be carried out as follows. Starting from an electrode separation corresponding to a state below the linear stability threshold, the distance d is gradually increased while the voltage ϕ is kept constant, the system being allowed to reach the purely conductive state at each step. Moreover, the injection is considered to be non-autonomous, following a field-dependent law as given by Felici & Gosse (1979) (see also Pontiga *et al.* 1995):

$$q_0 = \frac{q^*}{2bK_1(2b)}, \tag{18}$$

where q_0 is the charge density in C m^{-3} at the injector, q^* a constant linearly dependent on the residual conductivity σ of the liquid, and K_1 is the modified Bessel function of

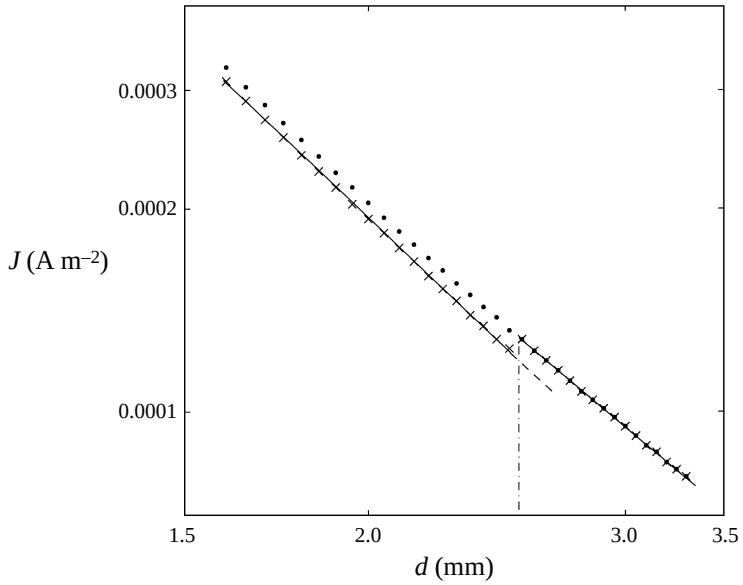

FIGURE 15. Current density as a function of the electrode separation for weak injection, corresponding to a solution of TIAP in cyclohexane ($\epsilon_r \approx 2.02$, $\eta \approx 0.96 \times 10^{-3}$ kg m^{-1} s^{-1}, $K \approx 1.3 \times 10^{-8}$ m^2 V^{-1} s^{-1}). The voltage is fixed at 10^4 V. Crosses and dots correspond to increasing and decreasing values of d, respectively.

the second kind and first order. The parameter b is the ratio of two physical distances, $b = L_B/L_E$, the Bjerrum distance $L_B = e^2/4\pi\epsilon k\theta$, where k is the Boltzmann constant and θ the absolute temperature, and the distance $L_E = (e/4\pi E(0))^{1/2}$ associated with the electric field at the injector.

The computer experiment was performed for a solution of TIAP in cyclohexane ($\epsilon_r \approx 2.02$, $\eta \cong 0.96 \times 10^{-3}$ kg m^{-1} s^{-1}), with residual conductivity $\sigma = 1 \times 10^{-11}\ \Omega^{-1}$ m^{-1} and mobility $K \approx 1.3 \times 10^{-8}$ m^2 V^{-1} s^{-1}, at 20 °C (Pontiga *et al.* 1995). The voltage is fixed at 10^4 V, which gives $T = 14331$. When the electrode separation d, which is initially set at 1 mm and corresponds to an injection strength $C = 0.059$, is increased, a critical value is reached at which the liquid is put into motion. This happens for $d = 2.55$ mm, as shown in figure 15, when the non-dimensional charge density at the injector is $C = 0.135$. Despite the large value of the average velocity amplitude reached by the liquid, $A = 9.1$, the jump in the current is relatively small, about 9.6% of the value of the current below the threshold. This small jump might explain the difficulties in detecting some evidence of the liquid motion from current measurements, and why the motion should be searched for by some direct procedure.

When the electrodes are brought nearer to below the critical threshold, there is no value of the distance d at which the steady hydrostatic state is recovered. The reason for this is that the parameter C never reaches a value low enough to lie below the nonlinear criterion for the given value of T. The dependence of C on d^2 is overcome by the high value of the electric field, and therefore of q_0, when the electrodes get closer. The hysteresis loop can be closed by choosing a lower value of T, i.e. of the voltage, in the experiment.

5. Conclusions

The development of a superparticle-type method to cope with the hyperbolic charge conservation equation makes it possible to overcome any inherent difficulties caused by the existence of sharp charge gradients, which are present in usual finite element and finite difference methods when applied to typical electrohydrodynamic problems. The method was applied successfully to the problem of finite-amplitude electroconvection in an insulating liquid layer. It was found that an accurate evaluation of Coulomb repulsion is essential to obtain time-dependent finite-amplitude electroconvection. The use of any simpler estimation, such as the analytical solution for the steady hydrostatic state, results in the extinction of any time variation in the computed liquid velocity and electrical current. A close link between the time fluctuations of velocity and current and the existence of a small amount of charge in some otherwise almost charge-free regions of the liquid was demonstrated.

All the well-known experimental features of electroconvection in the SCLC regime were satisfactorily reproduced, such as the linear and nonlinear criteria and the hysteresis loop in current–voltage characteristics, the size and spectral properties of current fluctuations, and the dependence of the characteristic frequency of the fluctuations on voltage.

Finite-amplitude electroconvection in the weak injection regime, where no conclusive experimental results are at present available, also shows some of the distinctive features present in the SCLC regime, although the range of frequencies to be explored is much higher than for SCLC (but still well within experimental possibilities). No difficulty was found in the application of the superparticle method when a realistic field-dependent injection law was considered instead of the simpler, but commonly assumed, autonomous injection.

The authors are indebted to Dr Alberto Pérez for many fruitful discussions. This work has been supported by the Spanish Dirección General de Investigación Cientifica y Técnica (DGICYT), under contracts PB93-1182, PB91-0570 and PB94-1139.

Appendix

Two points of practical importance must be considered in order to reduce the computation time to a minimum, given the large number of superparticles present in the system. One involves the localization algorithm of the four nearest neighbours to a superparticle, necessary for charge assignment and electric field interpolation. The other involves exceptional, though very many in practice, cases when a superparticle is not surrounded by four mesh points because it is close to the border of the computational cell. Setting special algorithms for these particular cases would result in a severe computational cost. The problem was solved by considering an, in some sense 'fictitous', extended mesh, which is constructed by adding to the real mesh two rows and two columns of new points outside the computational cell, symmetrically placed with respect to the borders with the corresponding inner mesh points. Using this extended mesh, any superparticle in the system is always surrounded by four extended-mesh points, and so the localization algorithm becomes general and straightforward. A superparticle located at (x, z) will belong to a rectangle $[x_i, x_{i+1}] \times [z_j, z_{j+1}]$ whose vertices are extended-mesh points, with $i = [(x + h_x/2)/h_x]$ and $j = [(z + h_z/2)/h_z]$, where $[x]$ means the integer part of x. Once the charge has been assigned to all the extended-mesh points, the charge attached to the outer points is merely transferred to its symmetric counterparts inside the computational cell.

Regarding the electric field interpolation at a superparticle position, the procedure is strictly analogous. To comply with the boundary conditions, E_x must change sign while E_z remains invariant when crossing the cell boundaries. The use of the extended mesh provides results in very good agreement with the analytical solution, at the same time keeping the computational cost within reasonable limits.

When the injection is strong a non-uniform computational mesh must be employed, as explained in the text. Since the gradients of charge density and electric field in the hydrostatic solution occur only along the z-coordinate, mesh uniformity will be retained in the horizontal direction. Therefore, the mesh will consist of $N_1 \times N_2$ cells, of equal horizontal size $h_x = L/N_1$ and variable height, being denser in the region near the injector and less so away from it. The most appropriate way of designing the variable mesh would be to keep the truncation error in the discretized Poisson equation of the same relative magnitude all across the cell. The size Δz of the mesh cells should then vary between the electrodes so that $\Delta q/q = \Delta z/(z+b) = \text{constant}$, as can easily be deduced from the analytical hydrostatic solution, with the value of the constant depending on the number N_2 of cells.

Even though construction of such a mesh is a very straightforward task, there is a serious disadvantage as regards the localization algorithm, due to the lack of any simple geometrical regularity. Hence, a different approach has been followed, with the height $h_z(j)$ of the j-row of mesh cells being taken to increase according to a geometrical growth factor α, $h_z(j) = h\alpha^j$, $j = 0, \ldots, N_2 - 1$, where h is the height of the cell next to the injector. Assuming that the truncation error in the discretized Poisson equation has the same relative magnitude at $z = 0$ and $z = 1$ immediately leads to the relationship $\Delta/h = (1+b)/b$, where $\Delta = h\alpha^{N_2-1}$ is the size of the cell next to the collector. Therefore, the number of vertical cells N_2 fixes the value of α. This, together with the condition that the distance between the electrodes is unity gives $h = (1-\alpha)/(1-\alpha\Delta/h)$.

The great advantage of using this mesh is that it makes it possible to obtain a simple and efficient algorithm to localize the four nearest neighbours to a superparticle located anywhere in the computational cell. Considering an extended mesh built in exactly the same way as in the weak injection case, a superparticle placed at (x, z) lies inside a rectangle $[x_i, x_{i+1}] \times [z_j, z_{j+1}]$ whose vertices are extended-mesh points, with

$$i = [(x + h_x/2)/h_x], \quad j = \text{ceil}\left[\frac{1}{\ln\alpha}\ln\left\{\frac{2}{\alpha+1}\left(1+\frac{\alpha-1}{h}z\right)\right\}\right], \tag{A 1}$$

where ceil$[x]$ refers to the minimum integer not less than x.

REFERENCES

Atten, P. 1996 Electrohydrodynamic instability and motion induced by injected space charge in insulating liquids. *IEEE Trans. Diel. Electr. Insul.* **3**, 1–17.

Atten, P. & Lacroix, J. C. 1979 Non-linear hydrodynamic stability of liquids subjected to unipolar injection. *J. Méc.* **18**, 469–510.

Atten, P., Lacroix, J. C. & Malraison, B. 1980 Chaotic motion in a Coulomb force driven instability: large aspect ratio experiments. *Phys. Lett.* A **79**, 255–258.

Atten, P. & Moreau, R. 1972 Stabilité électrohydrodynamique des liquides isolants soumis à une injection unipolaire. *J. Méc.* **11**, 471–520.

Castellanos, A. 1991 Coulomb-driven convection in electrohydrodynamics. *IEEE Trans. Electr. Insul.* **26**, 1201–1215.

Castellanos, A. & Atten, P. 1987 Numerical modelling of finite amplitude convection of liquids subjected to unipolar injection. *IEEE Trans. Ind. Appl.* **IA-23**, 825–830.

Castellanos, A., Atten, P. & Pérez, A. 1987 Finite amplitude electroconvection in liquids in the case of weak unipolar injection. *J. Physico-Chem. Hydrodyn.* **9**, 443–452.

Dennin, M., Treiber, M., Kramer, L., Ahlers, G. & Cannell, D. S. 1996 Origin of traveling rolls in electroconvection of nematic liquid crystals. *Phys. Rev. Lett.* **76**, 319–322.

Felici, N. 1969 Phénomenes hydro et aérodynamiques dans la conduction des diélectriques fluides. *Rev. Gén. Electr.* **78**, 717–734.

Felici, N. J. & Gosse, J. P. 1979 Injection d'ions par des électrodes métaliques dans les hydrocarbures liquides de résistivité élevée. *Rev. Phys. Appl.* **14**, 629.

Hockney, R. W. & Eastwood, J. W. 1981 *Computer Simulation using Particles*. McGraw-Hill.

Isaacson, E. & Keller, H. B. 1966 *Analysis of Numerical Methods*. Wiley.

Malraison, B. 1984 Transition vers le chaos et régimes chaotiques dans l'instabilité électro-hydrodynamique d'injection unipolaire. PhD Thesis, Université de Grenoble.

Malraison, B. & Atten, P. 1982 Chaotic behavior of instability due to unipolar ion injection in a dielectric liquid. *Phys. Rev. Lett.* **49**, 723–726.

Melcher, J. R. 1981 *Continuum Electromechanics*. MIT Press.

Pérez, A. T. & Castellanos, A. 1989 Role of charge diffusion in finite-amplitude electroconvection. *Phys. Rev.* A **40**, 5844–5855.

Pérez, A. T. & Castellanos, A. 1991 Laminar chaotic transport of charge in finite-amplitude electroconvection. *Phys. Rev.* A **44**, 6659–6664.

Pontiga, F., Castellanos, A. & Malraison, B. 1995 Some considerations on the instabilities of nonpolar liquids subjected to charge injection. *Phys. Fluids* **7**, 1348–1356.

Press, W. H., Flannery, B. P., Teukolsky, S. A. & Vetterling, W. T. 1986 *Numerical Recipes*. Cambridge University Press.

Schneider, M. & Watson, P. K. 1970 Electrohydrodynamic stability of space-charge-limited currents in dielectric liquids. I. Theoretical study. *Phys. Fluids* **13**, 1948–1954.